Ultraprecise studies of the thermal expansion coefficient of diamond using backscattering x-ray diffraction

Stanislav Stoupin and Yuri V. Shvyd'ko
Advanced Photon Source, Argonne National Laboratory, Argonne, Illinois 60439, USA
(Received 6 November 2010; published 17 March 2011)

The linear thermal expansion coefficient of diamond crystals of type IIa and type Ia was measured in the temperature range from 10 to 295 K. Neither negative thermal expansion nor any substantial difference in the thermal expansion coefficient in crystals of the different types were observed. An empirical expression was obtained that approximates the temperature dependence of the thermal expansion coefficient of diamond. The T^3 temperature dependence of a Debye solid holds below $\approx$100 K with an accuracy of $\approx 10^{-8}$ K^{-1}. A slight increase in the value of the lattice parameter was found for the Ia-type crystal, which suggests lattice dilatation by nitrogen impurity. The measurements were performed using Bragg diffraction in backscattering from diamond crystals of highly monochromatic 23.7 keV x rays with the recently demonstrated high relative accuracy of 1.2×10^{-8} in the determination of the lattice parameter [S. Stoupin and Yu. Shvyd'ko, Phys. Rev. Lett. **104**, 085901 (2010)].

DOI: 10.1103/PhysRevB.83.104102 PACS number(s): 65.40.De, 61.72.S−, 61.05.cp

I. INTRODUCTION

Diamond is a crucial material for many branches of modern technology. A growing number of demanding applications rely on the unique properties of diamond. For example, x-ray optics for next-generation synchrotron sources is facing a new challenge: to provide diffracting crystals stable under the extremely bright incident x rays.[1–4] Diamond is the primary candidate for this application due to its high radiation hardness, low x-ray absorption, record high thermal conductivity, and record high reflectivity for hard x rays in Bragg diffraction. To keep stable the Bragg reflection energy band of x rays, it is important to minimize the thermal variation of the crystal lattice parameter. This can be accomplished by cooling to cryogenic temperatures where the linear thermal expansion coefficient of diamond drops by a few orders of magnitude with respect to its room temperature value of $\simeq 1 \times 10^{-6}$. The knowledge of the thermal expansion coefficient allows quantitative evaluation of deviations in the lattice parameter $\delta a/a$ due to a variation in the crystal temperature δT. At temperatures around 40 K the coefficient becomes as small as $\frac{1}{a}\frac{\delta a}{\delta T} \approx 2 \times 10^{-9}$ K^{-1}, as reported recently.[5] For practical considerations, it is of special importance to verify the result by performing a series of experiments on diamond crystals of different type and origin with the best available accuracy. As a continuation of Ref. 5, here we present detailed studies of the thermal expansion in diamond.

The accuracy demonstrated in Ref. 5 in determination of lattice parameter $\Delta a/a \simeq 1.2 \times 10^{-8}$ is crucial for such an ultraprecise x-ray characterization of thermal expansion. Earlier experimental results of other groups[6–10] are based on the relative accuracy $\Delta a/a \approx 10^{-6}$ or more. For example, Haruna *et al.*[7,9,11] have measured the temperature-dependent lattice parameter of diamond using the Bond method[12] with an accuracy of about 1×10^{-6}. Values of the thermal expansion coefficient less than 10^{-8} K^{-1} at low temperatures have been predicted by polynomial extrapolation (i.e., have not been directly measured). Figure 1 summarizes experimental data on the thermal expansion coefficient of diamond reported in the literature prior to 2010.

Early theoretical studies discuss the possibility of negative thermal expansion (NTE) for diamond.[13,14] More recent theoretical works show that in contrast to Si and Ge, the effect does not exist for diamond because of the positive values of transverse-acoustic-mode Grüneisen parameters.[15,16] At the same time, low-concentration impurities in some crystals might cause low-temperature anomalies in the thermal expansion coefficient. It is also possible that some of these anomalies appear as the NTE effect.[17,18]

Given the importance of precise knowledge of the magnitude of thermal expansion of diamond for high-tech applications, its significance for understanding fundamental properties of solids, and the ability to perform ultraprecise measurements, further experimental studies are necessary. In this paper, we report the results of thermal expansion measurements for three high-quality IIa-type synthetic crystals from different manufacturers and for a crystal of type Ia. We show that contrary to previous studies,[9] temperature variation of the thermal expansion coefficients of these crystals can be approximated with a single empirical formula and that the deviation of the experimental values from the formula does not exceed 3×10^{-8} K^{-1} in the temperature range 10–295 K. The empirical formula deviates from the Debye T^3 approximation at temperatures of $\approx$200 K and above. No evidence of negative thermal expansion is found for any of the samples. An influence of impurities on the thermal expansion coefficient is not clearly manifested and thus remains speculative.

II. MEASUREMENT PRINCIPLES

The important role of x-ray Bragg backscattering in precision measurements was recognized awhile ago (e.g., Sachs and Weerts[19]). The technique was improved in the early 1970s when x-ray backsattering instruments for measuring relative changes of lattice parameters in crystals with an accuracy of 10^{-6} were built.[20–23] Further improvement in the measurement accuracy became possible with the use of monochromators with high energy resolution. High-energy-resolution Bragg diffraction in the backscattering configuration has been used

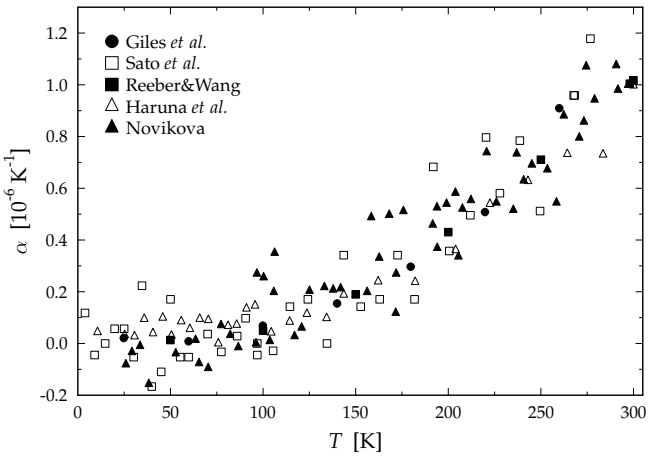

FIG. 1. Linear thermal expansion coefficient of diamond versus temperature: data from the literature prior to 2010. An experimental uncertainty of 5×10^{-7} K^{-1} reported by Giles *et al.*[10] is representative. Such uncertainty prevents direct measurements of the thermal expansion coefficient at temperatures $\lesssim$100 K.

to measure lattice parameters and x-ray wavelengths with high accuracy.[24–28]

The Bragg law in backscattering is

$$\lambda(1 + w) = 2d(1 - \Theta^2/2), \tag{1}$$

where λ is the wavelength of radiation reflected backward from a set of parallel atomic planes with interplanar distance d. In this equation, Θ is a small angular deviation from normal incidence to the reflecting planes; and w is the refraction correction, which is, to a good approximation a small invariant magnitude for a given set of atomic reflecting planes.[29] In the backscattering configuration, the influence of the angular variations $\delta\Theta$ on λ is minimized due to the Θ^2 dependence. If $\Theta \leqslant \sqrt{2\epsilon}$, where ϵ is the required relative uncertainty of measurements, a direct relation between the radiation wavelength and the interplanar distance can be established: $\lambda(1 + w) = 2d$.

However, any Bragg reflection and the incident radiation both have finite spectral widths. Only the central wavelength of the reflected x rays satisfies Eq. (1). The precision in measuring the interplanar distance is determined by several factors: the intrinsic spectral width ΔE of the chosen Bragg reflection, the bandwidth of the incident x rays ΔE_X, and the statistics with which the reflection is measured in the experiment.

III. EXPERIMENTAL

High quality diamond single crystals were preliminarily studied using white-beam x-ray topography performed at the X19C beamline of the National Synchrotron Light Source (Brookhaven National Laboratory). These studies provided information on crystal orientation and quality. Locations of stacking faults, dislocations, and inclusions were identified. Four diamond crystals with substantial defect-free areas were preselected for studies of thermal expansion. Samples C_1,C_2, and C_3 were synthetic high-pressure high-temperature (HPHT) crystals of IIa-type from different manufacturers: Sumitomo (Japan), Element Six (USA), and the Technological Institute for Superhard and Novel Carbon Materials (TISNCM, Russia), respectively. Sample C_4 was manufactured by Delaware Diamond Knifes (DDK, USA) and was of type Ia. The main characteristics of these crystals are given in Table I. Diamond single crystals of type IIa are classified as those that do not reveal infrared absorption due to boron impurity. The nitrogen impurity content is low for these crystals ($\lesssim$1 ppm). Diamonds of type Ia contain nitrogen impurities predominantly in the form of aggreagates (see, e.g., Ref. 30 for details). Nitrogen concentrations vary from $\approx$10 ppm up to 3000 ppm.

TABLE I. Characteristics of the studied diamond crystals.

	C_1	C_2	C_3	C_4
Type	IIa	IIa	IIa	Ia
Manufacturer	Sumitomo	Element Six	TISNCM	DDK
Orientation	(111)	(100)	(100)	(111)
Thickness	0.4 mm	0.4 mm	1.0 mm	0.2 mm
Reflection	(995)	(13 3 3)	(13 3 3)	(995)
ΔE	2.8 meV	2.7 meV	2.5 meV	3.7 meV
a (Å)	3.567 12(2)	3.567 12(2)	3.567 12(2)	3.567 16(2)

X-ray diffraction backscattering experiments were performed at the undulator beamline XOR 30-ID at the Advanced Photon Source at Argonne National Laboratory. The experimental setup is shown in Fig. 2. A highly monochromatic x-ray beam with an energy bandwidth of $\Delta E_X \simeq 1$ meV obtained using a consecutive application of a high-heat-load monochromator and a high-resolution monochromator (HRM) was incident on a diamond crystal. High-order reflections C (9 9 5) for crystals with (111) surface orientation and C (13 3 3) for crystals with (100) surface orientation with spectral bandwidth of $\Delta E \approx 3$ meV were chosen. The expected theoretical values for the spectral bandwidth depend on the crystal thickness (see Table I).

The intensity of the reflected x rays was measured using an avalanche photodiode (APD) placed 10 m from the sample. The reflected beam was aligned on the APD as described in Appendix A assuring a small angular offset $\Theta \simeq 1.3 \times 10^{-4}$ with an accuracy $\delta\Theta \approx 3.5 \times 10^{-5}$. This produces a negligible uncertainty in the wavelength $\delta\lambda/\lambda \approx \Theta\delta\Theta \approx 4.6 \times 10^{-9}$.

The Bragg energy of exact backscattering for the chosen reflections ($E_H = hc/2d = 23.765$ keV) is within an energy range of a six-bounce HRM operated at the beamline.[31,32] The HRM provides a monochromatic x-ray beam with a bandwidth of $\Delta E_X \simeq 1$ meV in the energy range 23.7–29.7 keV. The relative spectral resolution of this instrument is thus $\Delta E_X/E \simeq 4 \times 10^{-8}$, where $E = hc/\lambda$ is the photon energy. The precision for the measurement of a relative change in the central energy (or central wavelength) of a single diffraction peak is expected to be much better due to good counting statistics.

The HRM involves three pairs of diffracting crystals as shown in Fig. 2. The first pair (Si_1 and Si_2) consists of two asymmetric Si crystals using low-index Bragg reflections. The two crystals are coupled by a weak-link mechanism.[33] This pair is used to reduce the angular divergence of the x-ray beam to $\simeq$0.35 μrad, which is crucial for the monochromatization. The second pair (Si_3 and Si_4) is a liquid-nitrogen-cooled Si

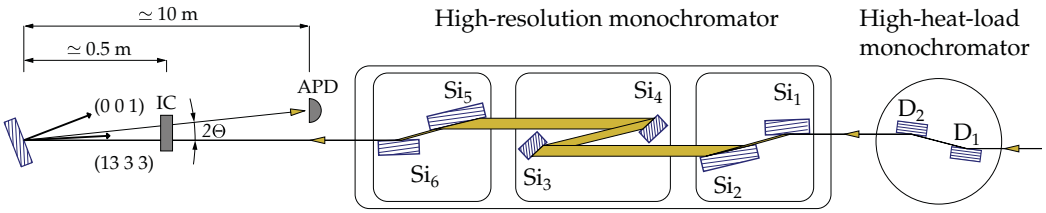

FIG. 2. (Color online) Experimental setup: A highly monochromatic x-ray beam with an energy bandwidth of $\Delta E_X \simeq 1$ meV obtained using a two-stage monochromatization process is incident on a diamond crystal. In the first stage, application of the high-heat-load monochromator produces x rays with an energy bandwidth of about 2 eV. In the second stage, the pre-monochromatized beam passes through the six-bounce high-resolution monochromator (HRM, crystals Si_{1-6}) to achieve the final bandwidth of $\simeq$1 meV.[31] The beam is reflected from either C (13 3 3) or C (9 9 5) atomic planes for samples with (100) and (111) orientation, respectively. The intensity of the reflected beam is measured using an APD detector placed next to the HRM at a distance of about 10 m from the sample. The choice of the large distance permits a small angular offset $\Theta = 1.3 \times 10^{-4}$ from normal incidence. The ion chamber (IC) facilitates searching of the reflected beam.

channel-cut[34] using high-index Bragg reflections and is the actual monochromator. The third crystal pair (Si_5 and Si_6) is similar to the first pair and is used to restore the size of the beam to the original size of the incident pre-monochromatized beam.

Monochromatization of x rays in the HRM is obtained using properties of Bragg reflections from two crystals in the dispersive configuration. A relative change of the central wavelength of the monochromatized beam is given by

$$\frac{\delta\lambda}{\lambda} = \frac{\delta\psi_{12}}{\tan\theta_1 + \tan\theta_2}, \tag{2}$$

where ψ_{12} is an angle between reciprocal vectors $\boldsymbol{H}_1$ and $\boldsymbol{H}_2$ of the Bragg reflections of the two crystals, and θ_1 and θ_2 are glancing angles of incidence to the first and the second crystals, respectively (see, e.g., Ref. 29 for details). In our setup, the crystal pairs $Si_{1,2}$ and $Si_{3,4}$ represent the aforementioned two crystals. The angle ψ_{12} is varied with an increment as small as 25 nrad.[31] Equation (2) is used to draw a correspondence between the angular scale of the monochromator and the energy of the resulting monochromatic x rays.

Initial measurements of reflectivity and the energy width ΔE were conducted at room temperature for different positions of the x-ray beam on each sample.[35] Crystal regions ($\approx 0.7 \times 0.7$ mm^2) were selected exhibiting a narrow and symmetric reflectivity curve. These regions were found to be within defect-free crystal areas in the corresponding white-beam x-ray topographs. For the sample C_4 the reflectivity of any region exhibited substantial broadening due to a lower crystalline quality. The best available region that exhibited a single reflectivity peak with narrowest width was chosen. The reflectivity curves of the selected regions for each crystal C_{1-4} are shown in Fig. 3 along with theoretical curves. The theoretical reflectivity was calculated using dynamical theory of x-ray diffraction for each diamond crystal of the given sample thickness and an incident x-ray beam with an energy bandwidth of 1 meV. The full width at half maximum (FWHM) of the experimental curves closely matches the theoretical results except for the type Ia crystal (C_4). For all crystals, variation of the FWHM of the reflectivity curves with temperature did not exceed 20%, which indicates that the probed regions were not developing strain in the course of all the measurements.

After the initial evaluation of each crystal, measurements of the relative change in the lattice parameter were performed as a function of temperature. The crystal was placed into a cryostat with a beryllium window to allow passage of the x rays. To

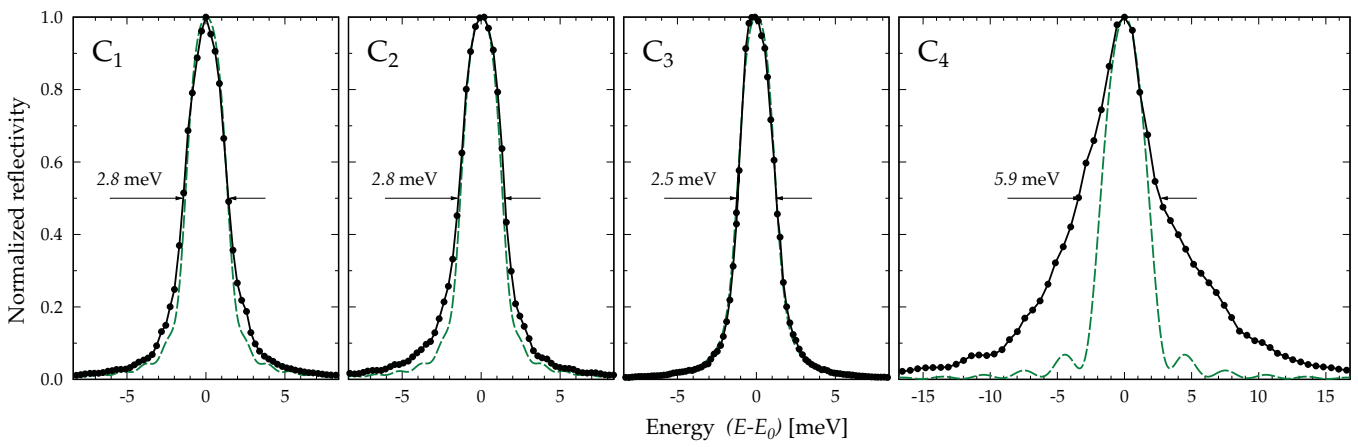

FIG. 3. (Color online) Normalized reflectivity curves from either (995) (C_1 and C_4) or (13 3 3) (C_2 and C_3) atomic planes: experimental curves for the selected region on each of the crystals (filled circles, solid black line); theoretical curves obtained using dynamical theory of x-ray diffraction for an incident x-ray beam with a bandwidth $\Delta E_X = 1$ meV (dashed lines).

obtain data for each experimental point, the temperature of the cryostat was lowered and allowed to equilibrate.

IV. RESULTS AND DISCUSSION

The absolute lattice parameter was determined for each sample using the procedure described in Appendix B. Equations (B6) and (B7) and experimental uncertainties yield the following lattice parameters at 298 K: $a_{\mathrm{IIa}} = 3.567\,12(2)$ Å for the crystals of type IIa, and $a_{\mathrm{Ia}} = 3.567\,16(2)$ Å for the crystal of type Ia (also given in Table I). Our value for a_{IIa} is in agreement with the result of Holloway *et al.*[36] [3.567 14(5) Å] and that of Yamanaka *et al.*[37] [3.567 11(5) Å] for diamond crystals with natural isotopic abundance. The lattice parameter of the type Ia diamond is larger by $(a_{\mathrm{Ia}} - a_{\mathrm{IIa}})/a_{\mathrm{IIa}} \approx 1 \times 10^{-5}$. Sato *et al.*[9] found a similar increase in the lattice parameter of a nitrogen-containing Ib-type diamond at room temperature. The increase was attributed to lattice dilatation due to substitutional nitrogen and was in agreement with the result of Lang *et al.*[38] for a sample containing 88 ppm nitrogen. The observed agreement in our case suggests a nitrogen concentration on the same order of magnitude, although contrary to aggregated nitrogen in type Ia, diamonds of type Ib contain single substitutional nitrogen as dominating defects.

The linear thermal expansion coefficients of the four crystals were obtained by point-by-point calculation. The resulting values are plotted in Fig. 4(a). The primary source of errors in the experiment is a limited reproducibility in mechanical motion of the ψ_{12} angular stage of the HRM. The statistical uncertainty $\Delta\psi_{12} = 0.1\ \mu$rad was the maximum observed mismatch between different statistical characteristics for the angular position of the reflectivity curve (e.g., position of the peak maximum vs the peak center of gravity). The experimental points were determined as peak positions of either Gaussian or Lorentzian profile fit to the experimental reflectivity curves measured at different temperatures.

Using Eq. (2) the statistical uncertainty yields $\delta a/a = 1.2 \times 10^{-8}$ as relative measurement accuracy of the lattice parameter. The size of the error bars in Fig. 4 is

$$\delta\alpha = \sqrt{2\left(\frac{1}{\Delta T}\frac{\delta a}{a}\right)^2 + \left(\alpha(T)\frac{\delta(\Delta T)}{\Delta T}\right)^2}. \tag{3}$$

The factor of 2 in the first root-mean-squared component of Eq. (3) reflects the fact that two measurements at neighboring temperature points T_1 and T_2 are required to obtain the value of the thermal expansion coefficient $\alpha(T)$, where $T = (T_1 + T_2)/2$. The second component represents uncertainty in determination of the temperature interval $\Delta T = T_2 - T_1$ between the experimental points. The inset in Fig. 4(a) shows the low-temperature regime $T \lesssim 100$ K where $\alpha(T) \lesssim 5 \times 10^{-8}$ K^{-1}. At these low temperatures the measured thermal expansion coefficient occasionally (i.e., no particular trend) takes small negative values; however, those remain within the experimental uncertainty ($\lesssim 4 \times 10^{-9}$ K^{-1}). Thus, negative thermal expansion is not observed in our experiment.

The solid line is an empirical formula,

$$\begin{aligned} x(T) &= bT^3 W(T) + cT^2[1 - W(T)], \\ W(T) &= \left(1 + \exp\frac{T - T_0}{\Delta T_0}\right)^{-1}, \end{aligned} \tag{4}$$

that approximates the measured linear thermal expansion coefficients of all four crystals simultaneously in the temperature range from 10 to 295 K. The parameters in Eq. (4) determined using least-squares fitting of all available data are given in Table II.

Deviations of the thermal expansion from the empirical formula $\Delta\alpha(T)$ are shown in Fig. 4(b) for each of the four samples. These deviations do not exceed 3×10^{-8} K^{-1} over the studied temperature range. The dotted line in Fig. 4(b)

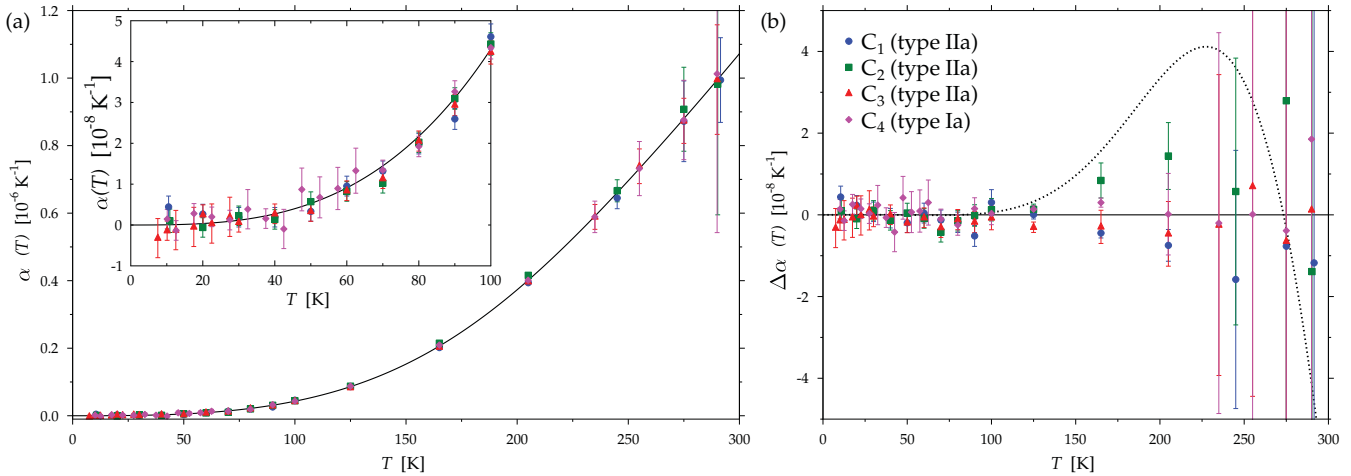

FIG. 4. (Color online) (a) Linear thermal expansion coefficients of IIa-type diamond crystals C_{1-3} and Ia-type C_4 obtained using point-by-point calculation from the results of the measurements. The notation of the symbols is the same as shown in the legend of the (b) panel. The solid line represents approximation with the empirical formula. The inset shows region of temperatures below 100 K in more detail. (b) Deviations of the measured thermal expansion coefficients from the empirical approximation. The dotted line is the difference between the empirical formula and the best fit to the Debye approximation (T^3).

TABLE II. Coefficients of the empirical formula Eq. (4) obtained using least-squares simultaneous fit of all available data.

Coefficient	Value
b	$3.6(6) \times 10^{-14}$ K^{-4}
c	$1.21(3) \times 10^{-11}$ K^{-3}
T_0	212(24) K
ΔT_0	47(5) K

represents the difference between the empirical formula and the best fit of all available data to the Debye approximation [$\alpha(T) = 4.25(2) \times 10^{-14} T^3$].

As an accurate representation of the thermal expansion coefficient, Eq. (4) illustrates a breakdown of the Debye approximation at temperatures about $T_0 = 212$ K, which is much less than $\Theta_D \simeq 2220$ K, the Debye temperature for diamond.[39] At temperatures $\lesssim$100 K, the thermal expansion coefficient is that of a Debye solid (T^3).

Our result for the thermal expansion coefficient at room temperature is in agreement with a value recommended earlier in several generalized studies[8,40,41] [$\alpha = 1 \times 10^{-6}$ K$^{-1} \pm$ (10–15)%]. The accuracy of our data is superior, i.e., $\alpha = 1.06(3) \times 10^{-6}$ K^{-1} at 300 K according to Eq. (4). A number of experimental studies report a somewhat higher value at room temperature. For example, the result of Sato *et al.*[9] for type IIa diamond is $\alpha = 1.6 \times 10^{-6}$ K^{-1}, yet the accuracy is not explicitly stated.

The presence of impurities, even at small concentrations ($\lesssim$10 ppm),[17,18] may alter the thermal expansion coefficient of a crystalline solid. Although a higher concentration of impurities is expected in the studied Ia-type diamond (C_4), this does not result in a measurable change of the thermal expansion coefficient. In our earlier work[5] we speculate that the increase in the thermal expansion coefficient observed for sample C_1 at $T \lesssim 20$ K could be attributed to tunneling effects due to low-concentration impurities/vacancies. However, to date we have not accumulated a sufficient data to either prove or disprove this hypothesis.

In the vicinity of room temperature our finding contradicts the results by Sato *et al.*,[9] where reduced values of the thermal expansion coefficient were found for $\lesssim$100 ppm nitrogen-doped and $\approx$100 ppm boron-doped diamonds with respect to that of a IIa-type specimen. This was attributed to an increase in the bulk modulus due to impurities. On the other hand, Brazhkin *et al.* found that an appreciable change in the thermal expansion of boron-doped diamonds occurs only at concentrations $>1\%$.[42] To address this controversy a more detailed ultraprecise experimental study is required, a study on doped crystals with dopant concentration characterized independently. Nevertheless, the present study offers an unambiguous ultraprecise result for the thermal expansion coefficient of single crystal diamond with small ($\lesssim$100 ppm) impurity concentrations.

V. CONCLUSIONS

In summary, ultraprecise measurements of the thermal expansion of diamond reveal the absence of a negative thermal expansion in the low temperature region (10 K $\lesssim T \lesssim$ 100 K) with a measurement accuracy of $\approx 10^{-9}$ K^{-1}. We conclude that as suggested in one of the early experimental studies on the topic by Novikova,[6] the effect of negative thermal expansion cannot be considered as a physical phenomenon characteristic of diamond crystals. Thus, the theoretical results[15,16,43–45] are now confirmed by direct measurements. Small negative values and faint trends reported earlier in literature can be attributed to the lack of measurement accuracy and possibly to the presence of impurities, which can alter the thermal expansion coefficient (e.g., tunneling effects).

Crystals of two different types were studied. Three of the samples were high-quality crystals of type IIa from different manufacturers and one crystal of type Ia of lower quality and with an increased impurity content. Indirect measurements of the absolute lattice parameter show an increased value for the Ia-type crystal, which is consistent with earlier observations interpreted as dilatation of diamond by an impurity. The result for the thermal expansion is essentially the same for all studied samples as approximated with a single empirical formula. Contrary to the findings of Sato *et al.*,[9] no difference in thermal expansion was found for the two different types of diamond crystals with different concentrations of nitrogen impurities. The empirical law is in agreement with thermal expansion of a Debye solid (T^3) at low temperatures ($\lesssim$100 K). The accuracy of the obtained approximation is $\simeq 3 \times 10^{-8}$ K^{-1} in the temperature range 10–295 K. With this accuracy, the presence of low-concentration impurities in the Ia-type sample does not alter the thermal expansion coefficient.

ACKNOWLEDGMENTS

We thank K.-J. Kim for stimulating interest and discussions. The help of our colleagues T. Roberts, A. Said, T. Gog, and X. Huang is greatly appreciated. We are indebted to R. Winarski and V. Blank for providing diamond crystals. T. Toellner and D. Shu are acknowledged for the development of the high-resolution monochromator. B. Raghothamachar is acknowledged for support in white-beam topography studies. We also thank C. P. Herrero and P. K. Schelling for helpful discussions on the topic. Use of the Advanced Photon Source, an Office of Science User Facility operated for the US Department of Energy (DOE) Office of Science by Argonne National Laboratory, was supported by the US DOE under Contract No. DE-AC02-06CH11357. Use of the National Synchrotron Light Source, Brookhaven National Laboratory, was supported by the US Department of Energy, Office of Science, Office of Basic Energy Sciences, under Contract No. DE-AC02-98CH10886.

APPENDIX A: ALIGNMENT PROCEDURE

The cryostat was mounted onto a θ-χ-ϕ goniometer with χ and θ being the angles in the horizontal and vertical planes, respectively. The ion chamber (IC) positioned at $\approx$0.5 m from the sample facilitated alignment of the reflected x rays on the APD detector as follows. The goniometer angles χ and θ were consecutively scanned in angular ranges where the Bragg condition at a chosen energy is fulfilled two times. The backscattering signal was recorded with the ion chamber. The resulting χ and θ scans, each containing two diffraction

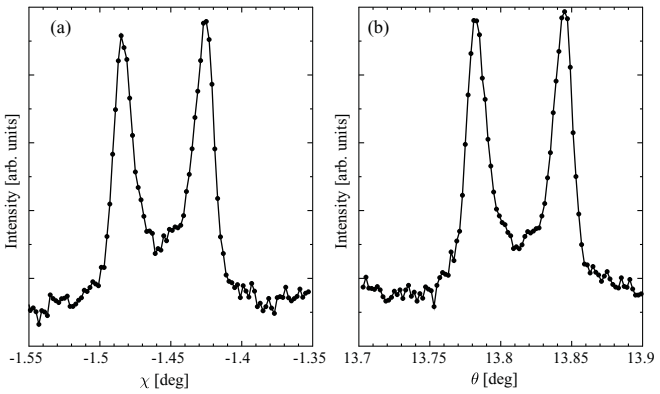

FIG. 5. Backscattering signal from the ion chamber as a function of χ (rotation in the plane perpendicular to the diffraction plane) (a) and the diffraction angle θ (b). At a chosen energy, the Bragg condition is fulfilled two times. For each scan the angle of the exact backscattering is approximated with the average angular position of the two peaks.

peaks, are shown in Fig. 5. Angles of the exact backscattering χ_0 and θ_0 were estimated as average angular positions of the two diffraction peaks. While $\chi = \chi_0$ was chosen, an angular deviation from the exact backscattering $\Theta \simeq 1.3 \times 10^{-4}$ was introduced to direct the reflected beam to the APD detector.

APPENDIX B: DETERMINATION OF THE LATTICE PARAMETER

Absolute measurement of the lattice parameter in our experiment required a reference on the energy/wavelength scale of the HRM (i.e., the angular scale of the cooled channel cut). The reference value was obtained by tuning the energy of the HRM to backscattering from a Si (12 12 12) analyzer at room temperature. Since Bragg reflections from Si at different temperatures are involved in the measurement, the knowledge of temperature dependence of the Si lattice parameter was required to perform the calibration. An empirical formula of Okada and Tokumaru[46] was chosen:

$$a^{\mathrm{Si}}(T) = a_0^{\mathrm{Si}}\left[\int_{T_0}^{T} \alpha^{\mathrm{Si}}(T)dT + 1\right],$$

$$\alpha^{\mathrm{Si}}(T) = A_1\{1 - \exp[-A_2(T - T_0)]\} + A_3 T, \quad \text{(B1)}$$

where a_0^{Si} is the lattice parameter at $T_0 = 273.2$ K, $A_1 = 3.725 \times 10^{-6}$, $A_2 = 5.88 \times 10^{-3}$, $A_3 = 5.548 \times 10^{-10}$, and $T_1 = 124$ K. This formula describes the temperature variation of the lattice parameter for high-quality Si and is applicable in the temperature range from 120 K to 1500 K. In the temperature range 120–300 K the formula is based on experimental data of Lyon *et al.*[47]

The Bragg law was applied to backscattering from the analyzer crystal and to the backscattering from a diamond crystal. In each of these cases the wavelength of the incident radiation was expressed using the Bragg law in the general form applied to the working reflection of the channel cut:

$$\lambda(1 + w_2) = 2d_2 \sin\theta_2, \quad \text{(B2)}$$

where d_2 is the interplane distance at 124 K, θ_2 is the glancing angle of incidence to the atomic planes, and w_2 is the refraction correction.

Backscattering from the atomic planes with the interplanar distance d_{Si} of the Si analyzer yields

$$\lambda(1 + w_{\mathrm{Si}}) = 2d_{\mathrm{Si}}\left(1 - \Theta_{\mathrm{Si}}^2/2\right). \quad \text{(B3)}$$

Here, w_{Si} is the refraction correction, and Θ_{Si} is the angular deviation from the exact backscattering.

Initially, the HRM was tuned to the backscattering from the Si (12 12 12) planes of the analyzer. The output intensity was maximized and the backscattering signal was recorded while scanning θ_2. The backscattering signal reached its maximum at a certain angular position of the θ_2 motor, which we denote as ρ_1. Under these conditions, the region of wavelengths selected by the HRM is centered at λ defined by Eq. (B2), and this wavelength also satisfies Eq. (B3). Thus, the unknown glancing angle of incidence θ_2^{Si} at which the analyzer backscattering is observed can be related to the characteristics of a Si crystal:

$$\sin\theta_2^{\mathrm{Si}} = \frac{d_{\mathrm{Si}}}{d_2}\frac{1 + w_2}{1 + w_{\mathrm{Si}}}\left(1 - \Theta_{\mathrm{Si}}^2/2\right). \quad \text{(B4)}$$

Similarly, the HRM was tuned to the diamond reflection of interest, and the maximum of the backscattering signal was observed at the motor position ρ_2. Application of the Bragg law as in the previous case yields the following expression for the interplanar distance of the diamond crystal:

$$d_{\mathrm{C}} = \frac{d_2 \sin\theta_2^{\mathrm{C}}}{1 - \Theta_{\mathrm{C}}^2/2}\frac{1 + w_{\mathrm{C}}}{1 + w_2}, \quad \text{(B5)}$$

where θ_2^{C} is the glancing angle of incidence for the channel cut at which the HRM is tuned to the diamond backscattering, w_{C} is the refraction correction, and Θ_{C} is the deviation from the exact backscattering. The difference between the actual θ_2 angles corresponding to backscattering from Si and diamond is equal to that of the motor positions: $\theta_2^{\mathrm{C}} - \theta_2^{\mathrm{Si}} = \rho_2 - \rho_1 = \Delta\rho$. Using this relationship, we calculate the interplanar distance for diamond from the Si crystal characteristics and the known experimental parameters:

$$d_{\mathrm{C}} = \frac{d_2 \sin\left[\theta_2^{\mathrm{Si}} + \Delta\rho\right]}{1 - \Theta_{\mathrm{C}}^2/2}\frac{1 + w_{\mathrm{C}}}{1 + w_2}. \quad \text{(B6)}$$

The lattice parameter was obtained as

$$a = d_{\mathrm{C}}\sqrt{n^2 + k^2 + l^2}, \quad \text{(B7)}$$

where n, k, and l are the Miller indices of the studied reflection.

[1] E. L. Saldin, E. A. Schneidmiller, Y. V. Shvyd'ko, and M. V. Yurkov, Nucl. Instrum. Methods Phys. Res. A **475**, 357 (2001).
[2] Y. Ding, Z. Huang, and R. D. Ruth, Phys. Rev. Phys. ST Accel. Beams **13**, 060703 (2010).
[3] G. Geloni, V. Kocharyan, and E. Saldin, Tech. Rep. DESY 10-133, DESY; e-print arXiv:1008.3036v1.
[4] K.-J. Kim, Y. Shvyd'ko, and S. Reiche, Phys. Rev. Lett. **100**, 244802 (2008).

[5]S. Stoupin and Y. V. Shvyd'ko, Phys. Rev. Lett. **104**, 085901 (2010).
[6]S. I. Novikova, Fiz. Tverd. Tela (Leningrad) **2**, 1617 (1960) [Sov. Phys. Solid State **2**, 1464 (1961)].
[7]K. Haruna, H. Maeta, K. Ohashi, and T. Koike, Jpn. J. Appl. Phys. **31**, 2527 (1992).
[8]R. R. Reeber and K. Wang, J. Electron. Mat. **25**, 63 (1996).
[9]T. Sato, K. Ohashi, T. Sudoh, K. Haruna, and H. Maeta, Phys. Rev. B **65**, 092102 (2002).
[10]C. Giles, C. Adriano, A. F. Lubambo, C. Cusatis, M. Irineu, and M. G. Hönnicke, J. Synch. Rad. **12**, 349 (2005).
[11]T. Saotome, K. Ohashi, T. Sato, H. Maeta, K. Haruna, and F. Ono, J. Phys. Condens. Matter **10**, 1267 (1998).
[12]W. L. Bond, Acta Cryst. **13**, 814 (1960).
[13]G. Dolling and R. A. Cowley, Proc. Phys. Soc. **88**, 463 (1966).
[14]S. Biernacki and M. Scheffler, Phys. Rev. Lett. **63**, 290 (1989).
[15]C. H. Xu, C. Z. Wang, C. T. Chan, and K. M. Ho, Phys. Rev. B **43**, 5024 (1991).
[16]P. Pavone, K. Karch, O. Schütt, W. Windl, D. Strauch, P. Giannozzi, and S. Baroni, Phys. Rev. B **48**, 3156 (1993).
[17]C. R. Case, K. O. McLean, C. A. Swenson, and G. K. White, AIP Conf. Proc. **3**, 183 (1972).
[18]C. R. Case and C. A. Swenson, Phys. Rev. B **9**, 4506 (1974).
[19]G. Sachs and J. Weerts, Z. Phys. **64**, 344 (1930).
[20]V. E. Bottom and R. A. Carvalho, Rev. Sci. Instrum. **42**, 196 (1970).
[21]B. Sykora and H. Peisl, Z. Angew. Phys. **30**, 320 (1970).
[22]A. Freund and J. Schneider, J. Cryst. Growth **13-14**, 247 (1972).
[23]A. Okazaki and M. Kawaminami, Jpn. J. Appl. Phys. **12**, 783 (1973).
[24]Y. V. Shvyd'ko, M. Lerche, J. Jäschke, M. Lucht, E. Gerdau, M. Gerken, H. D. Rüter, H.-C. Wille, P. Becker, E. E. Alp *et al.*, Phys. Rev. Lett. **85**, 495 (2000).
[25]H.-C. Wille, Y. V. Shvyd'ko, E. Gerdau, M. Lerche, M. Lucht, H. D. Rüter, and J. Zegenhagen, Phys. Rev. Lett. **89**, 285901 (2002).
[26]Y. V. Shvyd'ko, M. Lucht, E. Gerdau, M. Lerche, E. E. Alp, W. Sturhahn, J. Sutter, and T. S. Toellner, J. Synch. Rad. **9**, 17 (2002).
[27]M. Lucht, M. Lerche, H.-C. Wille, Y. V. Shvyd'ko, H. D. Rüter, E. Gerdau, and P. Becker, J. Appl. Cryst. **36**, 1075 (2003).
[28]M. Y. Hu, H. Sinn, A. Alatas, W. Sturhahn, E. E. Alp, H. C. Wille, Y. V. Shvyd'ko, J. P. Sutter, J. Bandaru, E. E. Haller *et al.*, Phys. Rev. B **67**, 113306 (2003).
[29]Y. V. Shvyd'ko, *X-Ray Optics. High Energy Resolution Applications* (Springer, Berlin, 2003).
[30]A. M. Zaitsev, *Optical Properties of Diamond: A Data Handbook* (Springer, Berlin, 2001).
[31]T. Toellner *et al.* (unpublished).
[32]S. Stoupin, F. Lenkszus, R. Laird, K. Goetze, K.-J. Kim, and Y. Shvyd'ko, Rev. Sci. Instrum. **81**, 055108 (2010).
[33]D. Shu, T. S. Toellner, and E. E. Alp, Nucl. Instrum. Methods. Phys. Res. A **467-468**, 771 (2001).
[34]T. S. Toellner, A. Alatas, A. Said, D. Shu, W. Sturhahn, and J. Zhao, J. Synchrotron Radiat. **13**, 211 (2006).
[35]Y. V. Shvyd'ko, S. Stoupin, A. Cunsolo, A. Said, and X. Huang, Nature Phys. **6**, 196 (2010).
[36]H. Holloway, K. C. Hass, M. A. Tamor, T. R. Anthony, and W. F. Banholzer, Phys. Rev. B **44**, 7123 (1991).
[37]T. Yamanaka, S. Morimoto, and H. Kanda, Phys. Rev. B **49**, 9341 (1994).
[38]A. R. Lang, M. Moore, A. P. W. Makepeace, W. Wierzchowski, and C. M. Welbourn, Phil. Trans. R. Soc. London A **337**, 497 (1991).
[39]K. A. Gschneidner Jr., in *Solid State Physics*, Vol. 16, edited by F. Seitz and D. Turnbull (Academic Press, New York, 1964), pp. 275–426.
[40]G. A. Slack and S. F. Bartram, J. Appl. Phys. **46**, 89 (1975).
[41]*Handbook of Industrial Diamonds and Diamond Films* (Marcel Dekker Inc., New York, 1998).
[42]V. V. Brazhkin, E. A. Ekimov, A. G. Lyapin, S. V. Popova, A. V. Rakhmanina, S. M. Stishov, V. M. Lebedev, Y. Katayama, and K. Kato, Phys. Rev. B **74**, 140502 (2006).
[43]C. P. Herrero and R. Ramírez, Phys. Rev. B **63**, 024103 (2000).
[44]P. K. Schelling and P. Keblinski, Phys. Rev. B **68**, 035425 (2003).
[45]N. Mounet and N. Marzari, Phys. Rev. B **71**, 205214 (2005).
[46]Y. Okada and Y. Tokumaru, J. Appl. Phys. **56**, 314 (1984).
[47]K. G. Lyon, G. L. Salinger, C. A. Swenson, and G. K. White, J. Appl. Phys. **48**, 865 (1977).